RSC Advances

This is an *Accepted Manuscript*, which has been through the Royal Society of Chemistry peer review process and has been accepted for publication.

Accepted Manuscripts are published online shortly after acceptance, before technical editing, formatting and proof reading. Using this free service, authors can make their results available to the community, in citable form, before we publish the edited article. This *Accepted Manuscript* will be replaced by the edited, formatted and paginated article as soon as this is available.

You can find more information about *Accepted Manuscripts* in the Information for Authors.

Please note that technical editing may introduce minor changes to the text and/or graphics, which may alter content. The journal's standard Terms & Conditions and the Ethical guidelines still apply. In no event shall the Royal Society of Chemistry be held responsible for any errors or omissions in this *Accepted Manuscript* or any consequences arising from the use of any information it contains.

ROYAL SOCIETY OF CHEMISTRY

www.rsc.org/advances

A first principle study on the spin transport properties in the heterojunctions based on zigzag-edged graphene nanoribbons and graphitic carbon nitrides nanoribbons

Xiangru Kong,[1] Dongqing Zou,[1] Hui Wang,[1] Xiaohui Jiang,[2] Sun Yin,[1] Dongmei Li,[1] and Desheng Liu[1,2,a]

[1] *School of Physics, State Key Laboratory of Crystal Materials, Shandong University, Jinan 250100, Peoples Republic of China*

[2] *Department of Physics, Jining University, Qufu 273155, Peoples Republic of China*

(Dated: 16 July 2015)

By using nonequilibrium Green's functions (NEGF) and density functional theory (DFT), we investigate the spin-dependent electronic transport properties of two heterojunctions based on zigzag-edged graphene nanoribbons and graphitic carbon nitrides nanoribbons. The only difference is the scattering region, i.e., one is zigzag-edged graphene nanoribbons (ZGNRs) and the other is graphitic carbon nitrides (g-C3N4) nanoribons. The I-V curves in the ferromagnetic and antiferromagnetic states for both devices are demonstrated. Our results show that the heterojunctions are promising multifunctional devices in molecular spintronics due to the nearly perfect spin-filtering efficiency (SFE) and high rectification ratio (RR). Spin negative differential resistance (SNDR) properties at low biases can also be found in the two devices. The mechanisms are proposed for these phenomenons. The spin polarizations in the transmission spectrums result in the nearly perfect SFE, the asymmetry in the structures gives rise to the high RR. Moreover, for the SNDR, the suppression of transmission spectrums caused by the localization in total density of states is the main reason.

[a] Author to whom correspondence should be addressed. Electronic mail:liuds@sdu.edu.cn

RSC Advances Accepted Manuscript

Molecular spintronics,[1,2] which combines molecular electronics and spintronics together, aims to manipulate the electron's spin degree as well as the charge degree in molecular devices. The switching of the parallel or antiparallel magnetization direction between the two magnetic electrodes in the prototypical giant magnetoreistance (GMR) device inspired the construction of the spin-related electronic devices.[3] The magnetic properties of the electrodes and the molecule sandwiched between them are important on the behaviors of the spin-related molecular devices. Hence, it is utmost important to choose suitable magnetic materials to construct spin-related multifunctional molecular devices in molecular spintronics. For two-dimensional (2D) materials flexibility in artificial manipulation and potential electronic properties for the application in electronic components,[4–6] the success in pursuit of graphene[7] undoubtedly opened up a field in the research of the graphene-like 2D materials. According to the edge characteristics, cutting a single layer of graphene sheet will normally form two types of graphene nanoribbons (GNRs): armchair-edged GNRs (AGNRs) and zigzag-edged GNRs (ZGNRs). ZGNRs have attracted increasing interest for its magnetic properties. Its ground state is regarded as the two edge states antiferromagnetically coupled[8] and this coupling could be tuned to be ferromagnetic by applying magnetic field.[9,10] Rectification and amplification of spin-polarized current is reported in the pristine ZGNRs-based devices.[11] On the other hand, the introduction like chemical doping[12] and vacancy[13] in pristine ZGNRs-based devices could result in other interesting magnetic properties, such as SNDR.[14] Considering graphene-based monolayer devices should be supported on an excellent substrate, g-C3N4 has been used to synthesize a hybrid graphene/g-C3N4 nanocomposite by experimentalists.[15] For its optically active properties, g-C3N4 is regarded as a potential candidate for optoelectronic devices.[16] Since then, graphitic carbon nitrides as one of the graphene-like 2D materials have attracted considerable attention.[17,18] The electronic structures of g-C3N4 differs significantly from those of graphene. Spin-polarization and ferromagnetism behaviors were also found in the modified tri-s-triazine based g-C4N3.[19] This indicates g-C3N4 may also be a promising material in molecular spintronics, especially in nanoribbon structure.

To explore the interfacial electronic structure of the hybrid graphene/g-C3N4 nanocomposite, Du *et al.* proposed that the nanocomposite displayed significant charge transfer from graphene to the g-C3N4 substrate and the energy gap opened by the strong electronic coupling shed light on the construction of field effect transistors.[20] Until now, the spin-dependent

RSC Advances Accepted Manuscript

transport properties of the monolayer devices of graphene and g-C3N4 have not been studied and whether the hererojunctions are potential nanoelectronics devices is unclear. In the present work, we propose two heterojunctions based on ZGNRs and s-triazine-based g-C3N4 nanoribbons. The scattering region in one device is ZGNRs and the other is g-C3N4. The spin-dependent results such as nearly perfect SFE, high RR and SNDR indicate our devices have promising application in future nanoelectronics. The interesting results also demonstrate ZGNRs and g-C3N4 are qualified as electrodes and scattering region in the construction of nanoelectronics devices.

The nanostructured hererojunctions referred as GGN and GNN are shown in Fig. 1(a) and (b), respectively. The left electrode is semi-infinite ZGNRs and the right electrode is s-triazine-based g-C3N4 nanoribbons. The central scattering region is divided into three parts as shown in the figure by the label GGNA, GGNB and GGNC (GNNA, GNNB and GNNC). The only difference between the two devices is located in GGNB (ZGNRs) and GNNB (g-C3N4 nanoribbons). The geometry optimizations and the electronic transport properties are calculated by the *ab initio* code package Atomistix ToolKit (ATK), which is based on the combination of density functional theory (DFT) with the non-equilibrium Green's function (NEGF) technique.[21] The single zeta polarization basis set is used for all atoms in our constructed devices. The cutoff energy is set to 150 Ry and the mesh grid of the k space is 1×1×100. The exchange-correlation potential takes the form of the Perdew-Zunger parametrization of the local spin density approximation (LSDA) which works well in previous works.[22–25]

According to NEGF formulas, the spin-dependent currents through the scattering region are calculated by the Landauer-like formula[26]

$$I_\sigma(V_b) = \frac{e}{h}\int_{\mu_r(V_b)}^{\mu_l(V_b)} T_\sigma(E,V_b)[f_l(E,V_b) - f_r(E,V_b)]dE \qquad (1)$$

Here, $\sigma = \uparrow$ (spin up) and $\sigma = \downarrow$ (spin down), $T_\sigma(E,V_b)$ is the bias-dependent and spin-dependent transmission coefficient, $f_{l(r)}(E,V_b)$ is the Fermi−Dirac distribution function of the left (right) electrode. $\mu_{l(r)}(E,V_b)$ is the electrochemical potentials corresponds to the left or right electrode. Considering the fact that the Fermi level is set to zero, the region of the energy integral window $[\mu_l(E,V_b),\ \mu_r(E,V_b)]$ can be written as $[-V_b/2,\ V_b/2]$.

In our work, the spin density distributions of our structures in the ferromagnetic (FM) state are shown in Fig. 1(c)-(f). For the spin density distribution of ZGNRs, we could

RSC Advances Accepted Manuscript

observe the strong edge effect and ferromagnetic coupled properties in Fig. 1(c). For the g-C3N4 nanoribbons in our calculation, Fig. 1(f) shows that it manifests obvious ferromagnetic properties and the spin density distribution on the nitrogen atoms of the lower edge indicates the edge effect in g-C3N4 nanoribbons. Fig. 1(d) and (e) represent the spin density distributions of our constructed hererojunctions. The edge effect maintains strong in the ZGNRs part. The part of ZGNRs closes to the g-C3N4 nanoribbons part has a suppression of spin density distribution, especially in the upper edge. The lower edge's larger spin density distribution of our devices indicate it will be the main spatial transport channel. On the other hand, the correlative structures with nitrogen atoms terminated by hydrogen atoms in the lower edge of g-C3N4 part are shown in Fig. 2.[27] The devices are labeled by HGGN and HGNN, respectively. Compared with the spin density distributions in Fig. 1(f), it can be concluded that hydrogenation will suppress the edge effect of the g-C3N4 part and weakens the magnetism as shown in Fig.2 (d). From Fig. 2(c) and (e), the spin density distributions in the lower edge of g-C3N4 part disappear and this will make edge effect for the spin-dependent transport properties of the correlative structures (HGGN and HGNN) less important (For the transport properties of HGGN and HGNN, please see the Section I in the supplementary materials).

In Fig. 3(a), (b) and (c), we show the transmission spectrums and total density of states (TDOS) of pristine ZGNRs device (GGG), GGN and GNN at zero bias, respectively. There are two obvious transmission peaks near the Fermi level in the device GGG and the corresponding TDOS peaks indicate the peaks origin from the edge states. The states below the Fermi level and above the Fermi level correspond to the spin up and spin down channel, respectively. The differences of the structures lead to the differences in the TDOS in devices GGN and GNN and this results in the obvious different transport properties in the devices as can be seen from transmission spectrums in Fig. 3(b) and (c). There are two wide peaks in the transmission spectrum near the Fermi level in device GGN. The spin up channel is farther from the Fermi level than the spin down channel. However, in device GNN the transmission spectrum near the Fermi level becomes more localized than GGN and more peaks appear. Also the spin up channel is farther from the Fermi level than the spin down channel in the device GNN.

From above, we could expect obvious different transport properties in devices GGN and GNN. Here, we consider both the ferromagnetic (FM) and antiferromagnetic (AFM) states.

RSC Advances Accepted Manuscript

The I-V curves in the FM state are shown in Fig. 4 (a) and (b). Obvious SNDR phenomenon can be observed in the positive bias ranges in both devices. For device GGN, both spin channels behave NDR properties but start at different biases, i.e., 0.3V for the spin up channel and 0.5 V for the spin down channel. In the bias range of 0-0.4V, the magnitude of the current in the spin down channel is larger than that in the spin up channel. For device GNN, we can conclude only the spin down channel behave obvious NDR property and start at bias 0.4V. The magnitude of the current in the spin down channel is larger than that in the spin up channel in the bias range of 0-0.7V. The nearly perfect SFE can be observed in both devices and the polarizability is shown in the insets (k1) and (k4). At zero bias, the SFE is defined as

$$SFE = \frac{T_{\downarrow}(E_f) - T_{\uparrow}(E_f)}{T_{\uparrow}(E_f) + T_{\downarrow}(E_f)} \tag{2}$$

where $T_{\uparrow}(E_f)$ and $T_{\downarrow}(E_f)$ represent the transmission coefficient of the up and down spin channel at the Fermi level, respectively. At finite bias, the SFE is defined as

$$SFE = \frac{I_{\downarrow}(V_b) - I_{\uparrow}(V_b)}{I_{\uparrow}(V_b) + I_{\downarrow}(V_b)} \tag{3}$$

where $I_{\uparrow}(V_b)$ and $I_{\downarrow}(V_b)$ respectively represent the magnitude of the up and down spin current at bias V_b. The nearly 100% SFE can be observed in the bias range of -0.4-0.2V in device GGN and high SFE above 87% can be found in the bias of -0.4-0.6V. Moreover, the RR is plotted in the insets (k2), (k3), (k5) and (k6). The largest RR in the spin down channel in device GGN is 24 while the RR above 4000 can be maintained in the spin up channel in the bias range of 0.3-0.4V. The largest RR in the spin down channel in device GNN can reach 126 while the RR above 800 can be maintained in the spin up channel in the bias range of 0.1-0.3V. The I-V curves in the AFM state for both devices are shown in Fig. 4 (c) and (d) (For spin density distributions, transmission spectrums and TDOS of both devices at zero bias in the AFM state, please see the Section II in the supplementary materials). The results show that the currents start at 0.2V in the AFM state for both devices and for both spin channels in the positive bias ranges. Starting from 0.6V, obvious NDR in the spin down channels appear in both devices. On the other hand, nearly perfect SFE can also be found in the AFM state for both devices in the negative bias ranges as can be seen in the insets (k7) and (k10). For the RR shown in the insets (k8), (k9), (k11) and (k12), the largest RR could be 886, 11, 153 and 48, respectively. On the below, we will understand the SNDR, nearly perfect SFE and high RR on the condition of the FM state.

RSC Advances Accepted Manuscript

To understand the SFE behavior, the transmission spectrum and the corresponding transmission pathways of devices GGN and GNN at bias 0.1 V are shown in Fig. 5. From Fig. 5 (a) and (b), we can observe in the bias window the spin down channel mainly contributes the conductance. Compared with Fig. 3 (b) and (c), the transmission spectrum moves closer to the Fermi level as the bias increases. The transmission pathways in Fig. 5 (c) and (e) indicate that the spin up channel is blocked completely. The contributions to the spin up transmission coefficient is localized on the left side of the hererojunctions. However, the spin down channel is unblocked in Fig. 5(d) and (f). The transmission pathways mainly go along the lower edge of the g-C3N4 part. This is due to the larger spin density distribution in the lower edge. So only the spin down current is observed and it results in nearly perfect SFE.

For the high RR behavior, we focus on the transport properties at bias 0.3V and -0.3V in both devices. The value of RR at this bias is 7369 for the spin up channel in device GGN, 14 for the spin down channel in device GGN, 1634 for the spin up channel in device GNN, 146 for the spin down channel in device GNN. Fig. 6 (a) and (b) indicate the conductance at bias 0.3V is larger than -0.3V. The transmission eigenstates in the spin up channel at bias -0.3V in Fig. 6 (c) and (d) is almost zero. This is not the case in the spin up channel at bias 0.3V. So the RR at bias 0.3V is very high. For the spin down channel in Fig. 6 (c) and (d), the transmission eigenstates are more localized on one side of the devices at bias -0.3 V than 0.3V. So the rectification behavior is observed but lower than the spin up channel.

For the SNDR behaviors, the NDR behavior in the down spin channel in the device GGN as shown in Fig. 4(a) is discussed typically in this work. In Fig. 7, we give the transmission spectrum, the DOS (TDOS, PDOS) of device GGN. The molecular projected self-consistant Halmitonian energy spectrum is shown in Fig. 7. At bias 0.1V, no energy level appear in the bias window and no transmission peak completely appear in the bias window. As the bias increases to 0.3V, two energy levels come close in the bias window in Fig. 8. In Fig. 7(b), two twin peaks in TDOS turn up in the bias window. At Fermi level, the GGNC part contributes the larger part in the TDOS and it can be verified in the inset of Fig.6 (b). It can be concluded that the DOS result in the suppression of transmission spectrum. But the conductance still strengths for the larger bias window. When the bias reaches 0.6V, more energy levels appear in the bias window. The TDOS becomes more localized. At -0.08 eV, there is a TDOS peak and the GGNB part contributes the most which can be seen in

RSC Advances Accepted Manuscript

the inset of Fig.6 (c). The localization in TDOS results in the localization of transmission spectrum. Though the bias window becomes larger, the conductance drops at the beginning of 0.3V. So the NDR behavior is observed.

In conclusions, through first-principle quantum transport calculations, we have shown the spin-related transport properties of two heterojunctions based on ZGNRs and g-C3N4 nanoribbons. Nearly perfect SFE, high RR and SNDR can be observed in our devices in the both ferromagnetic and antiferromagnetic states. The mechanism for the phenomenons are proposed in this work. Our results indicate ZGNRs and g-C3N4 have the potential applications in future nanoelectronics. The device which behaves rectification properties can be directly designed as NOT gate. The SFE and SNDR behaviors in our constructed devices also have the potential to be designed as logic gates. This truly demonstrates the promising application of our work in molecular spintronics.

ACKNOWLEDGMENTS

This work was supported by the Natural Science Foundation of China (Grant Nos. 11374183, 21473102, 11404141 and 11404188).

REFERENCES

[1] M. Ratner, Nature nanotechnology **8**, 378 (2013).

[2] S. Sanvito, Chemical Society Reviews **40**, 3336 (2011).

[3] G. Binasch, P. Grünberg, F. Saurenbach, and W. Zinn, Phys. Rev. B **39**, 4828 (1989).

[4] D. Golberg, Y. Bando, Y. Huang, T. Terao, M. Mitome, C. Tang, and C. Zhi, ACS Nano **4**, 2979 (2010), http://dx.doi.org/10.1021/nn1006495.

[5] H. Zhang, C.-X. Liu, X.-L. Qi, X. Dai, Z. Fang, and S.-C. Zhang, Nature physics **5**, 438 (2009).

[6] H. Tang, D. Liang, R. L. Qiu, and X. P. Gao, Acs Nano **5**, 7510 (2011).

[7] K. S. Novoselov, A. K. Geim, S. Morozov, D. Jiang, Y. Zhang, S. Dubonos, I. Grigorieva, and A. Firsov, science **306**, 666 (2004).

[8] Y. Niimi, T. Matsui, H. Kambara, K. Tagami, M. Tsukada, and H. Fukuyama, Physical Review B **73**, 085421 (2006).

RSC Advances Accepted Manuscript

[9]W. Y. Kim and K. S. Kim, Nature nanotechnology **3**, 408 (2008).

[10]F. Muñoz-Rojas, J. Fernández-Rossier, and J. Palacios, Physical review letters **102**, 136810 (2009).

[11]M. Zeng, L. Shen, M. Zhou, C. Zhang, and Y. Feng, Physical Review B **83**, 115427 (2011).

[12]G. Heimel, E. Zojer, L. Romaner, J.-L. Brédas, and F. Stellacci, Nano letters **9**, 2559 (2009).

[13]J. Palacios, J. Fernández-Rossier, and L. Brey, Physical Review B **77**, 195428 (2008).

[14]X. Kong, B. Cui, W. Zhao, J. Zhao, D. Li, and D. Liu, Organic Electronics **15**, 3674 (2014).

[15]Q. Xiang, J. Yu, and M. Jaroniec, The Journal of Physical Chemistry C **115**, 7355 (2011), http://dx.doi.org/10.1021/jp200953k.

[16]Y. Zhang, T. Mori, L. Niu, and J. Ye, Energy Environ. Sci. **4**, 4517 (2011).

[17]X. Li, Y. Dai, Y. Ma, S. Han, and B. Huang, Physical Chemistry Chemical Physics **16**, 4230 (2014).

[18]Y. Zheng, J. Liu, J. Liang, M. Jaroniec, and S. Z. Qiao, Energy & Environmental Science **5**, 6717 (2012).

[19]A. Du, S. Sanvito, and S. C. Smith, Physical review letters **108**, 197207 (2012).

[20]A. Du, S. Sanvito, Z. Li, D. Wang, Y. Jiao, T. Liao, Q. Sun, Y. H. Ng, Z. Zhu, R. Amal, and S. C. Smith, Journal of the American Chemical Society **134**, 4393 (2012), pMID: 22339061, http://dx.doi.org/10.1021/ja211637p.

[21]M. Brandbyge, J.-L. Mozos, P. Ordejón, J. Taylor, and K. Stokbro, Physical Review B **65**, 165401 (2002).

[22]T.-T. Wu, X.-F. Wang, M.-X. Zhai, H. Liu, L. Zhou, and Y.-J. Jiang, Applied Physics Letters **100**, 052112 (2012).

[23]C. Jiang, X.-F. Wang, and M.-X. Zhai, Carbon **68**, 406 (2014).

[24]Y. Ren and K.-Q. Chen, Journal of Applied Physics **107**, 044514 (2010).

[25]X. Deng, Z. Zhang, C. Yang, H. Zhu, and B. Liang, Organic Electronics **14**, 3240 (2013).

[26]M. Büttiker, Y. Imry, R. Landauer, and S. Pinhas, Physical Review B **31**, 6207 (1985).

[27]J. Zhang, X. Gong, B. Xu, Y. Xia, J. Yin, and Z. Liu, physica status solidi (b) **251**, 1386 (2014).

RSC Advances Accepted Manuscript

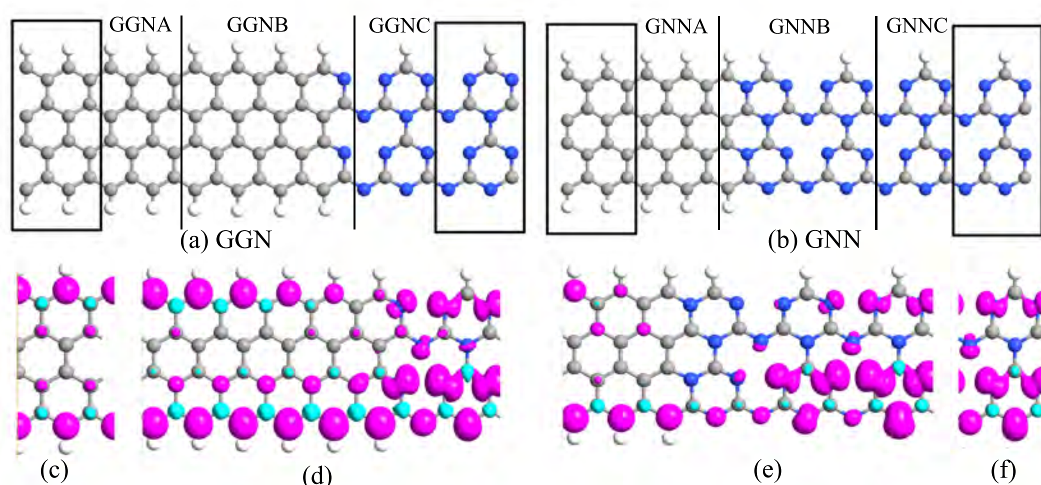

FIG. 1. (color online) (a) and (b) Correspond to the two heterojunctions based on ZGNRs and s-triazine-based g-C3N4. The rectangle regions represent the electrodes. (c) and (f) Correspond to the spin density distributions of ZGNRs and g-C3N4 in bulk configuration. (d) and (e) Correspond to the spin density distributions of our nanostructured hererojunctions.

RSC Advances Accepted Manuscript

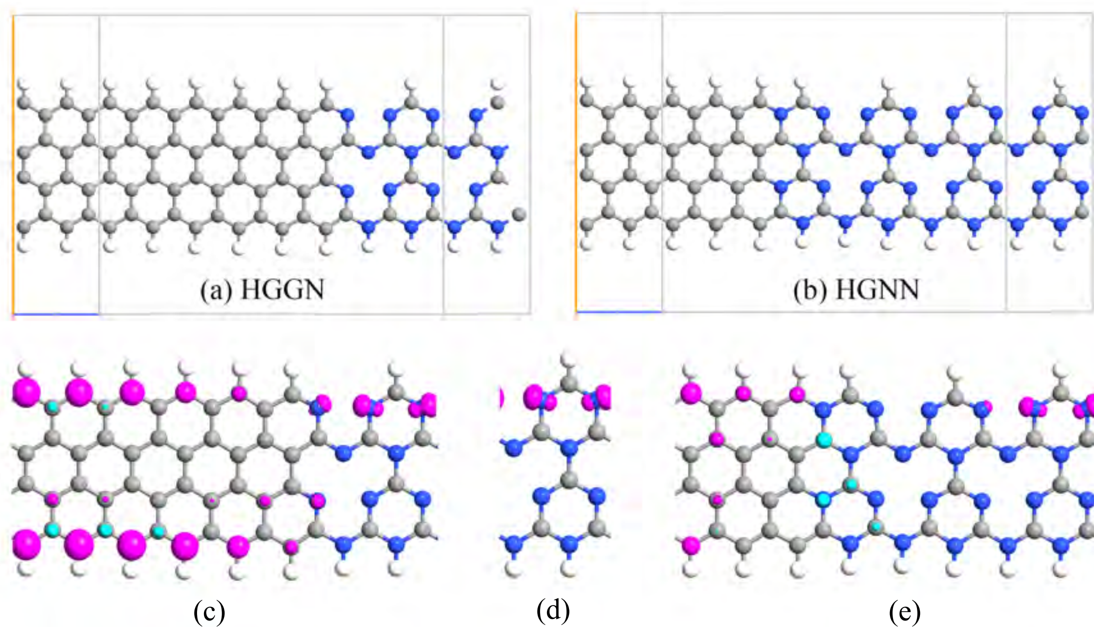

FIG. 2. (color online) (a) and (b) Correspond to the two heterojunctions based on ZGNRs and s-triazine-based g-C3N4 with nitrogen atoms terminated with hydrogen atoms. (c) and (e) Correspond to the spin density distributions of HGGN and HGNN. (d) Correspond to the spin density distributions of g-C3N4 with nitrogen atoms terminated with hydrogen atoms in bulk configuration.

RSC Advances Accepted Manuscript

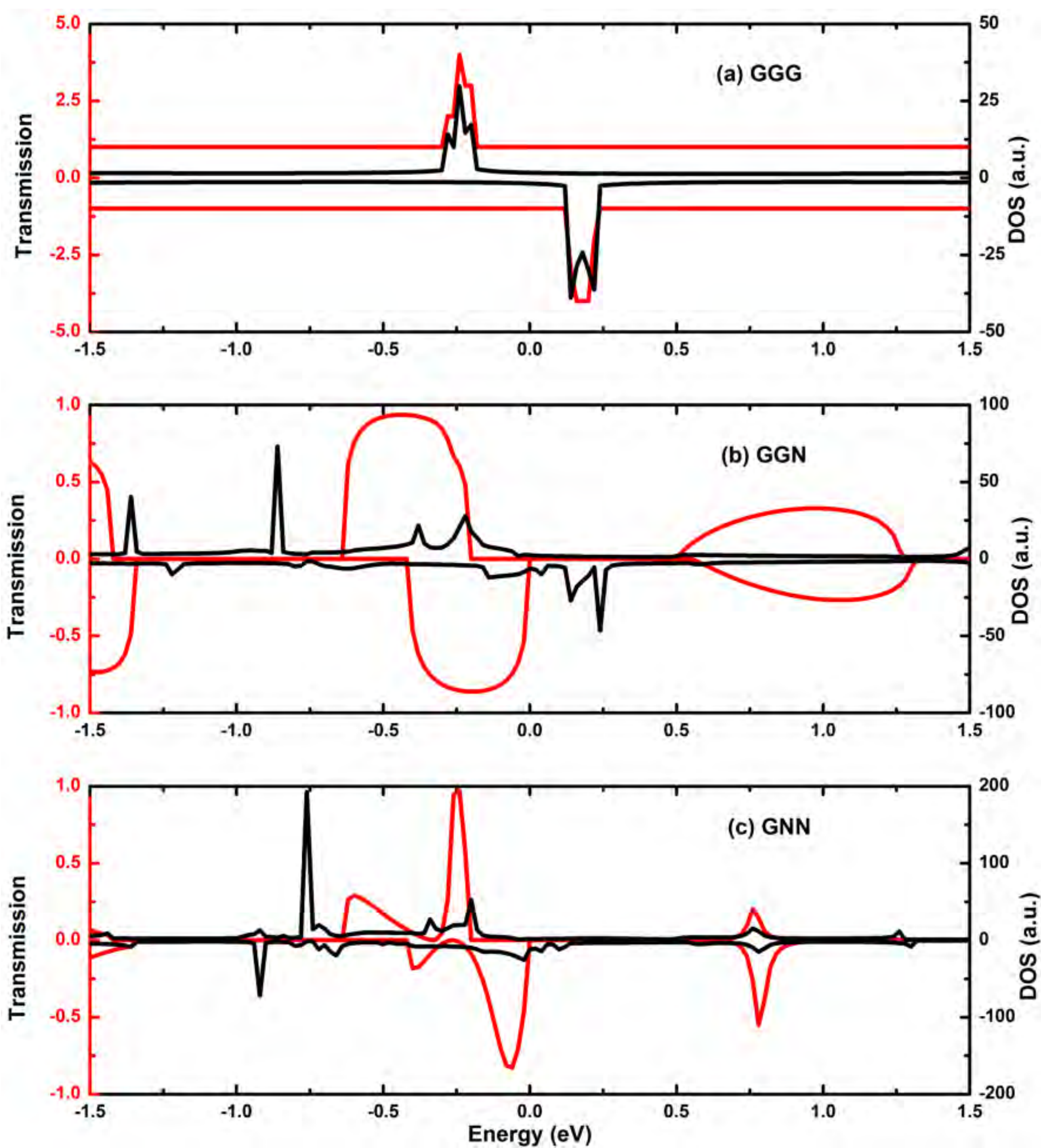

FIG. 3. (color online) The transmission spectrums and total density of states of (a) pristine ZGNRs device, (b) GGN and (c) GNN at zero bias. The red line represents the transmission spectrums and the black line represents the total density of states.

RSC Advances Accepted Manuscript

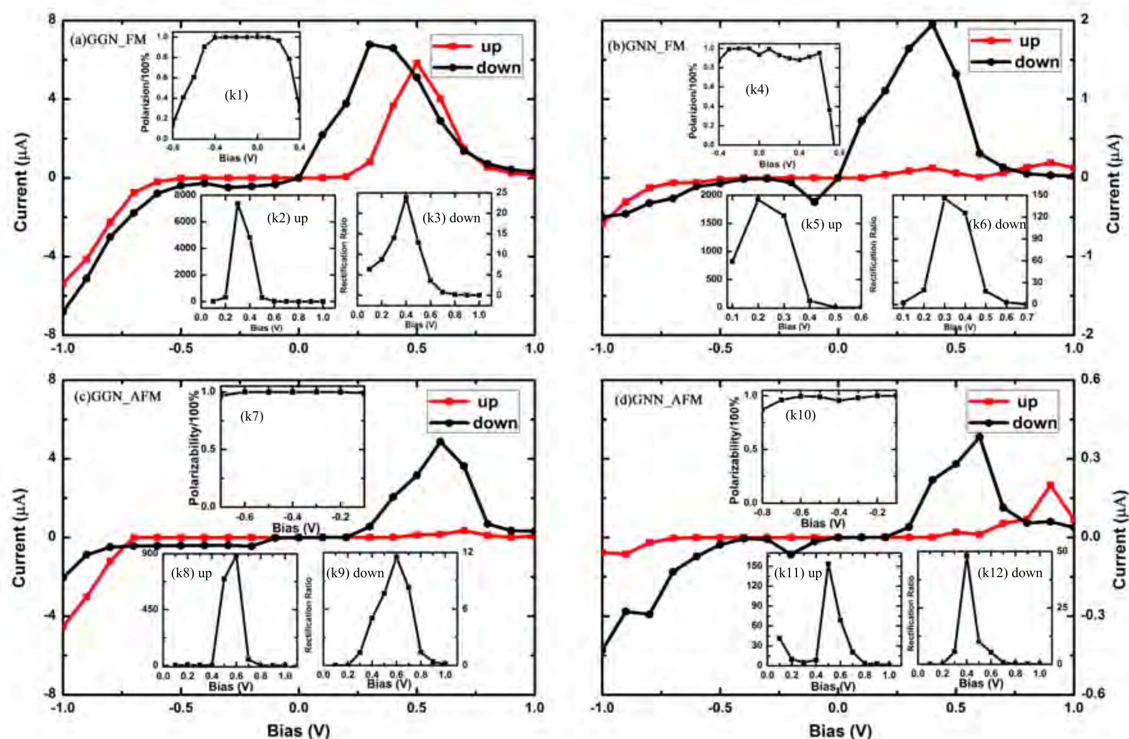

FIG. 4. (color online) (a), (b) Correspond to the I-V curves of device GGN and GNN for the ferromagnetic state, respectively; (c), (d) Correspond to the I-V curves of device GGN and GNN for the antiferromagnetic state, respectively. Insets: (k1),(k7) SFE in GGN; (k2),(k8) RR for the spin up channel in GGN; (k3),(k9) RR for the spin down channel in GGN; (k4),(k10) SFE in GNN; (k5),(k11) RR for the spin up channel in GNN; (k6),(k12) RR for the spin down channel in GNN.

RSC Advances Accepted Manuscript

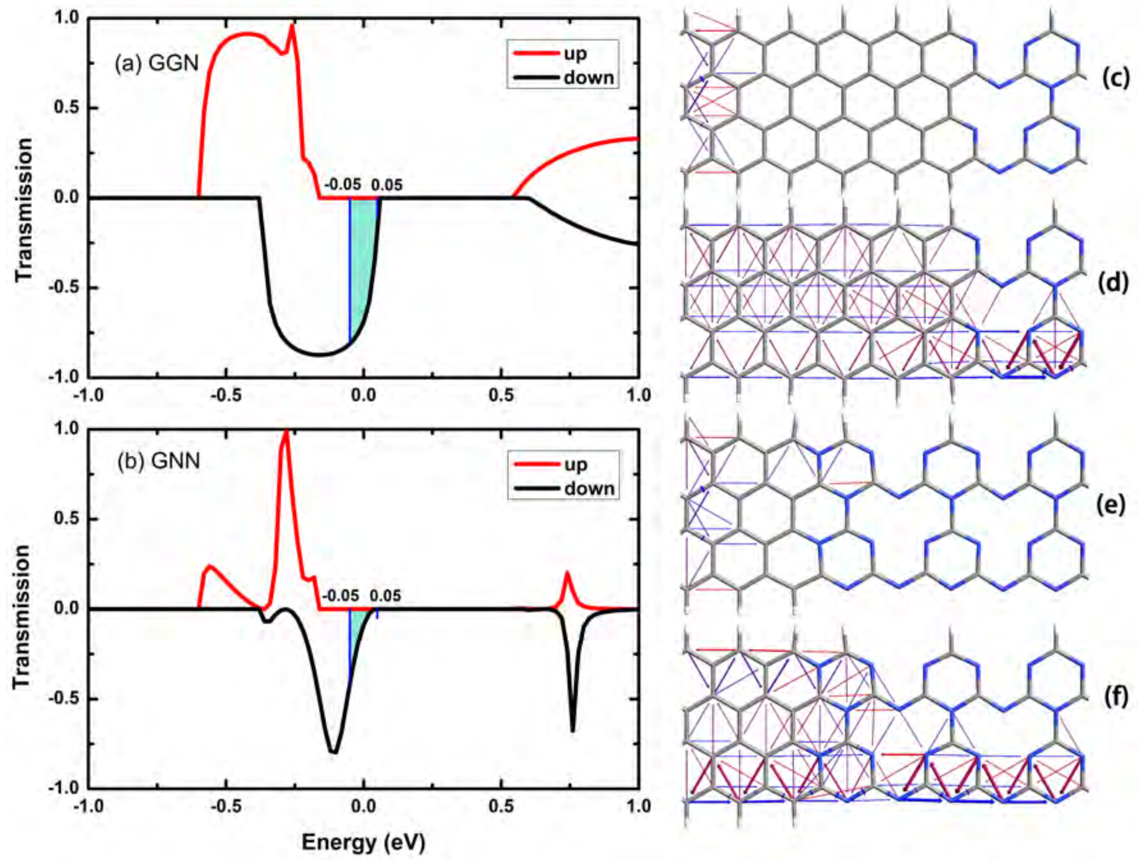

FIG. 5. (color online) The transmission spectrum of devices (a) GGN and (b) GNN at 0.1V. The corresponding transmission pathways of (c) spin up channel in GGN, (d) spin down channel in GGN, (e) spin up channel in GNN, (f) spin down channel in GNN. The blue lines indicate the bias window.

RSC Advances Accepted Manuscript

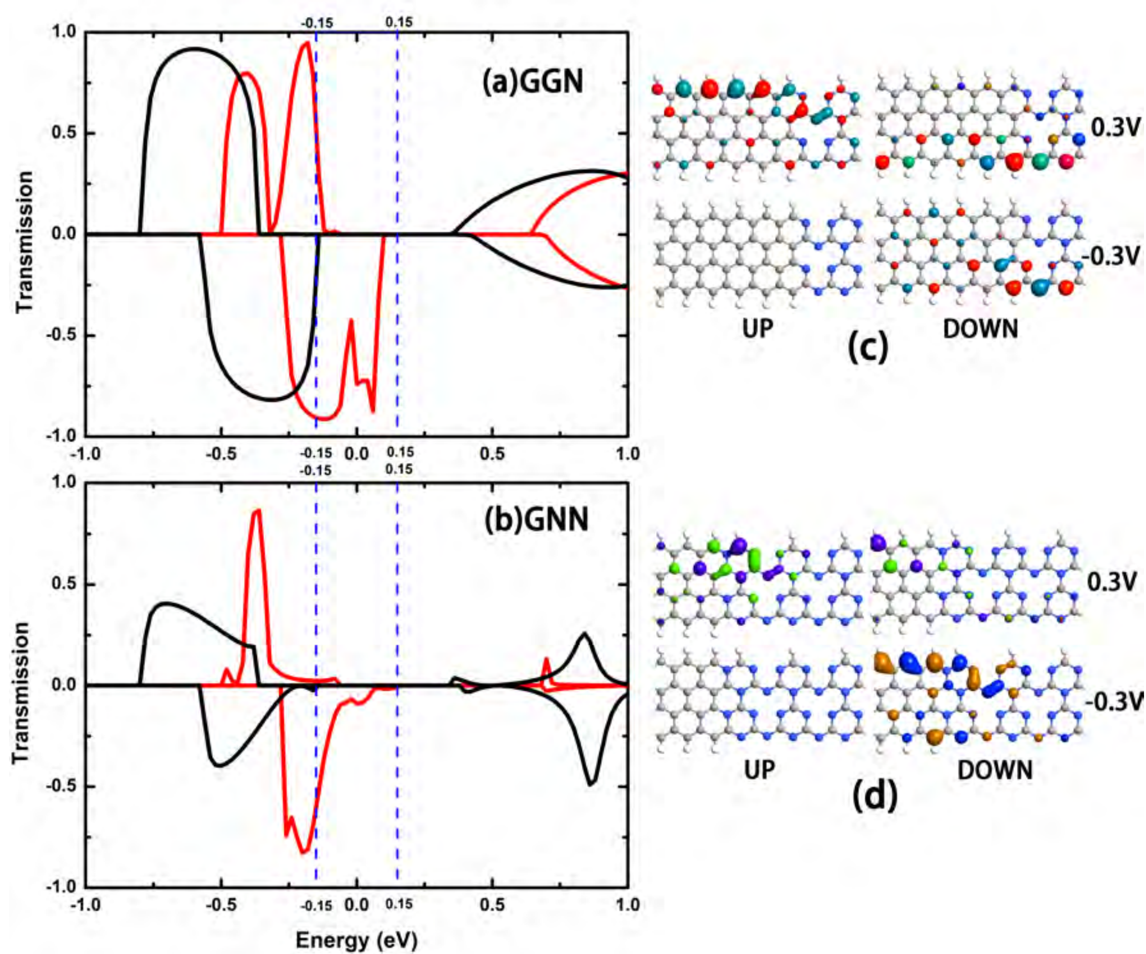

FIG. 6. (color online) The transmission spectrum (red line for 0.3V, black line for -0.3V) of devices (a) GGN and (b) GNN. (c), (d) Correspond to the corresponding transmission eigenstates at Fermi level. The blue dashed lines indicate the bias window.

RSC Advances Accepted Manuscript

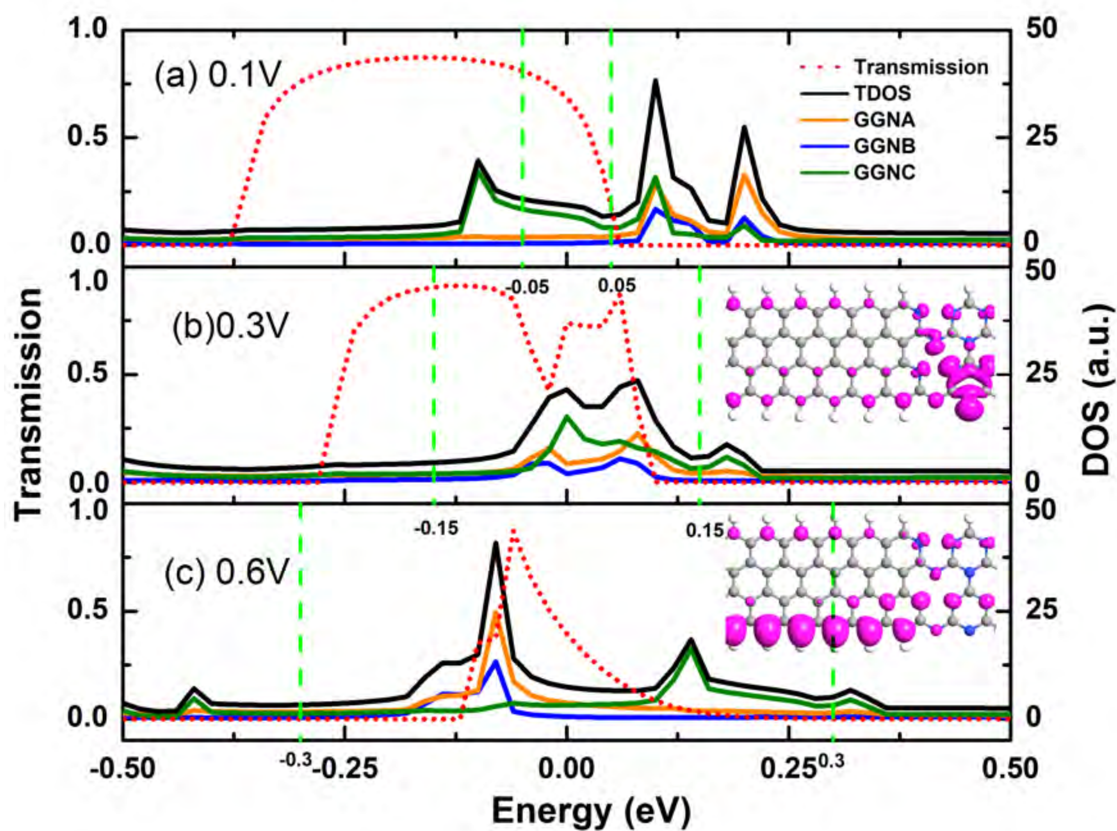

FIG. 7. (color online) The transmission spectrum, TDOS, the projected density of states (PDOS) of three parts labeled in Fig.1 (a) in device GGN at bias (a) 0.1V, (b) 0.3V and (c) 0.6V for the spin down channel. The inset in (b): the corresponding local density of states at Fermi level. The inset in (c): the corresponding local density of states at -0.08eV. The green dashed lines indicate the bias window.

RSC Advances Accepted Manuscript

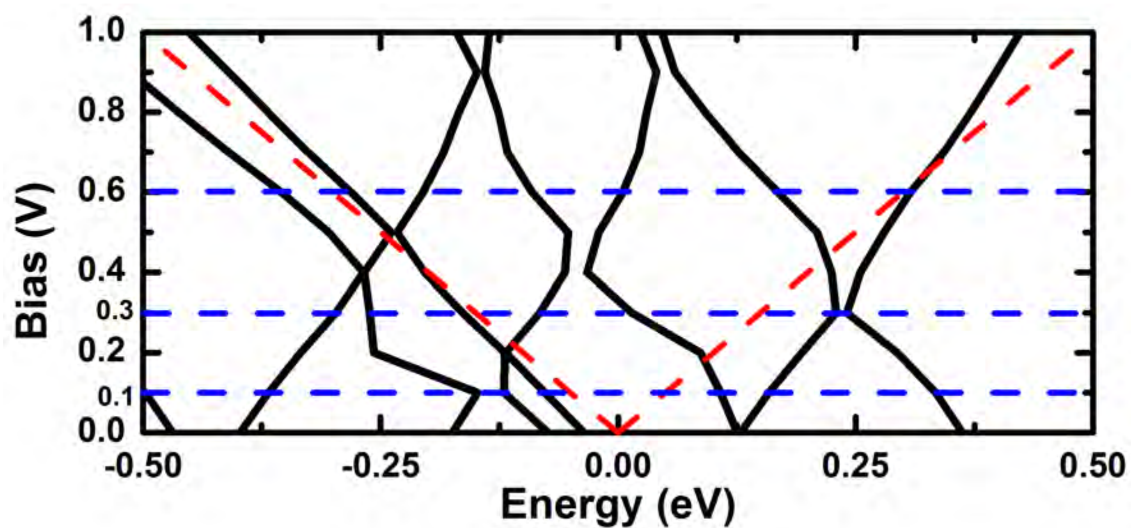

FIG. 8. (color online) The projected self-consistant Hamiltonian energy spectrum of device GGN. The red dashed lines indicate the bias window. The blue dashed lines indicate the biases of 0.1 V, 0.3 V and 0.6V.

RSC Advances Accepted Manuscript